Available online at www.sciencedirect.com

SCIENCE DIRECT®

PERGAMON

International Journal of Multiphase Flow 29 (2003) 1373–1394

International Journal of Multiphase Flow

www.elsevier.com/locate/ijmulflow

A stochastic description of wall sources in a turbulent field. Part 1: Verification

Yoichi Mito, Thomas J. Hanratty *

Department of Chemical and Biomolecular Engineering, University of Illinois, 205 Roger Adams Laboratory, Box C-3, 600 South Mathews Avenue, Urbana, IL 61801, USA

Received 18 February 2003; received in revised form 24 June 2003

Abstract

A stochastic model for the dispersion and deposition of particles in a turbulent field is explored. The trajectories of particles originating from a wall source in a horizontal channel are considered. The fluid turbulence seen by the particles is modeled by a Langevin equation that is modified to account for spatial nonhomogeneities. The results of these studies are used to describe a simplified version of an annular flow in which particles, admitted to the field at the two walls, mix and deposit downstream. In these calculations the walls are represented as arrays of point sources. The relative strengths of the sources at the two walls are adjusted so as to realize a stationary state. The results are compared with calculations done in a direct numerical simulation of the turbulence. Considering the simplicity of the model, the agreement is quite good. The work described in this paper opens the possibility of carrying out studies of the diffusion and deposition processes over a wide range of conditions. The development of a physical understanding of the concentration distribution and of the rate of deposition is of particular interest.

Keywords: Horizontal annular flow; Particle dispersion; Wall source; Turbulent channel flow; Lagrangian method; Langevin equation; Direct numerical simulation; Fully-developed concentration field

1. Introduction

Significant advances have been made in understanding the dispersion and deposition of solid spheres by solving the equation of motion in a direct numerical simulation (DNS) or a large eddy simulation (LES) of a turbulent field. Particle dispersion from a point source or from uniformly

* Corresponding author. Tel.: +1-217-333-1318; fax: +1-217-333-5052.
E-mail address: hanratty@scs.uiuc.edu (T.J. Hanratty).

0301-9322/$ - see front matter
doi:10.1016/S0301-9322(03)00138-1

distributed point sources in a channel flow has been studied by Brooke et al. (1994) and Chen and McLaughlin (1995) in a DNS and by Wang and Squires (1996) and Wang et al. (1997) in a LES of turbulent flow in a channel. Calculations in a DNS require large amounts of computer time, so they are restricted to small Reynolds numbers and to simple geometries. Such calculations are of limited usefulness in exploring a large range of system variables. Large eddy simulations offer some improvement but there are uncertainties in modeling the subgrid scale turbulence and fine grids must be used in the viscous wall layer when considering processes such as particle deposition. This paper explores an alternate computational method in which a modified Langevin equation is used to describe the fluid turbulence seen by the particles by testing the accuracy of the stochastic model against experiments done in a DNS.

The system being considered is a turbulent flow in a horizontal channel for which particles are admitted to the field by arrays of sources from both walls. Particles from a given instantaneous source are dispersed by turbulence and gravity; they, eventually, deposit on a wall. The relative rates of admitting the particles at the two walls are adjusted so that after a sufficient time a fully-developed concentration field is reached for which there is no change of the number of particles in the field. The basic problem, then, is the description of the behavior of an instantaneous source.

The contributions of this paper are as follows: (1) New results are presented for a wall source at $Re_\tau = 150$. (2) The accuracy of a stochastic model which uses the Langevin equation to define the fluid turbulence is examined. (3) The representation of a disperse flow as resulting from a distribution of sources is illustrated for an idealized version of an annular flow. (4) The deposition process that is examined differs from previous work (cited above) in that a stationary condition is considered, for which the rate of introducing particles equals the rate of deposition. In a subsequent paper (Part 2), the stochastic model is used at a larger Re_τ to examine the effects of the inertial time constant and the settling velocity on dispersion and deposition.

A modified Langevin equation has been developed to calculate dispersion of fluid particles in nonhomogeneous fields by Hall (1975), Reid (1979), Wilson et al. (1981), Legg and Raupach (1982), Durbin (1983, 1984), Thomson (1984, 1986, 1987), van Dop et al. (1985) and Reynolds (1997). Mito and Hanratty (2002) have exploited these advances to study fluid particle dispersion in a channel flow. They used results for dispersion from sources at different locations in a DNS to define the spatial variation of the Lagrangian time constant. Good agreement was obtained between experiments in a DNS and calculations with a modified Langevin equation that used a joint Gaussian forcing function.

The use of the Langevin equation to describe fluid velocities seen by a dispersing solid sphere has been explored by Perkins (1992) and by Pozorski and Minier (1998). Iliopoulos et al. (2003) considered turbulent flow in a channel. They used this approach to calculate dispersion and deposition of solid spheres originating from a source located at 40 wall units from the boundary and from point sources which are uniformly distributed over the channel cross section. Good agreement was noted between calculations done with a DNS and a Langevin model.

The motivation for the work described in the three parts of this paper is to study the relative effects of gravity and turbulence in horizontal annular flow. Because of gravity, the drops distribute asymmetrically and the rate of deposition is greater at the bottom wall. Under fully-developed conditions the rates of atomization and deposition are the same at each wall. In order to carry out the calculation it is necessary to specify how the particles enter the turbulent field. We have used the simple assumption that they are propelled from the wall with a constant velocity

having normal components of $V_2^+ = 1$ from the bottom and $V_2^+ = -1$ from the top, where the plus indicates that the velocity has been made dimensionless with the friction velocity.

The method of describing the concentration field as resulting from a distribution of wall sources and sinks is the same as used by Hanratty (1956) and by Papavassiliou and Hanratty (1997) to describe scalar transport. The important role of droplet mixing in the behavior of horizontal annular flows is emphasized in works of Paras and Karaberas (1991), Pan and Hanratty (2002) and Baik and Hanratty (2003).

2. Definition of the system

The simplified annular flow that is considered is depicted in Fig. 1. The flow is fully-developed. The drops are represented by solid spheres. The Reynolds number, $Re_\tau = 150$, is defined with the friction velocity, v^*, and the half-height of the channel. Particles are injected from the bottom wall at a rate R_{Ab} with a velocity $V_1^+ = 15$, $V_2^+ = 1$, $V_3^+ = 0$ and from the top wall at a rate R_{At} with a velocity $V_1^+ = 15$, $V_2^+ = -1$ and $V_3^+ = 0$. These velocities are representative of the turbulent velocities outside the viscous wall layer. They were chosen because we presume that particles can be entrained into the flow field only by strong turbulence events. Calculations show that the magnitude of the streamwise component of the injection velocity affects the streamwise distribution of particles emitted from a wall source. However, it has negligible effects on the distribution in the wall normal direction and on the deposition constant. For the τ_{p}^+ considered in this paper, the magnitude of the wall normal velocity of the injected particles has a negligible effect on the deposition constant at very small dimensionless gravities. However, its influence increases with increasing gravitational effects (This behavior is discussed in Part 2 of this paper). The particles are treated as points that deposit when they are at a distance of $d_{\mathrm{p}}/2$ from the wall, where d_{p} is the diameter of the particles. The rates of deposition at the bottom and top walls are designated by R_{Db} and R_{Dt}, where

$$R_{\mathrm{Ab}} = R_{\mathrm{Db}} \quad \text{and} \quad R_{\mathrm{At}} = R_{\mathrm{Dt}} \tag{1}$$

when a fully-developed condition is realized. The ratio $R_{\mathrm{At}}/R_{\mathrm{Ab}}$ is calculated from the following relation, given by Binder and Hanratty (1992):

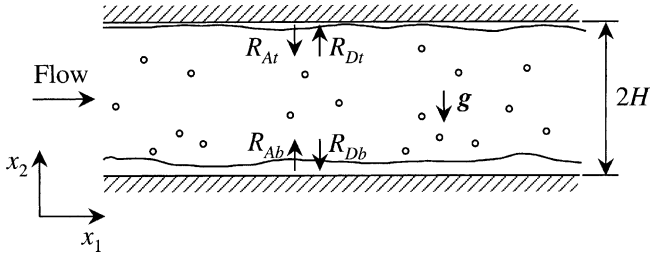

Fig. 1. Gas–liquid horizontal annular flow.

$$\frac{R_{At}}{R_{Ab}} = \frac{F_{bt}}{F_{tb}}, \tag{2}$$

where F_{bt} and F_{tb} are, respectively, the fraction of the particles that reached the top wall in the calculation of particle dispersion from a bottom wall source and the fraction of the particles that reached the bottom wall in the calculation of particle dispersion from a top wall source. When the gravitational effect is large, $R_{At} = R_{Dt} = 0$ and a film flow does not exist on the top wall.

The trajectories of the particles are calculated with the following equations:

$$\frac{dx_i}{dt} = V_i, \tag{3}$$

$$\frac{dV_i}{dt} = -\frac{3\rho_f C_D}{4 d_p \rho_p} |\boldsymbol{V} - \boldsymbol{U}|(V_i - U_i) + g_i, \tag{4}$$

where V_i is the velocity of a particle, U_i is the gas velocity seen by the particle, ρ_f is the density of the gas, ρ_p is the density of the particle, and g_i is a component of the acceleration of gravity. In the system shown in Fig. 1, $g_2 = -g$ and $g_1 = g_3 = 0$, where g is the magnitude of the acceleration of gravity. The drag coefficient, C_D, is given by

$$C_D = \frac{24}{Re_p}(1 + 0.15 Re_p^{0.687}), \tag{5}$$

(Clift et al., 1978) where the particle Reynolds number Re_p is defined with d_p and the magnitude of the relative velocity $|\boldsymbol{U} - \boldsymbol{V}|$. The gas velocity seen by the particle, U_i, is calculated from a DNS or a modified Langevin equation. The simplified equation of motion for the particles, Eq. (4), includes the effect of nonlinearities on the fluid drag but does not include the effects of lift or a correction for the fluid drag in the near-wall region. With the assumption that the concentrations of particles are small enough, particle/particle interactions and the influence of the particles on the fluid turbulence are ignored.

3. Description of the DNS

The DNS of fully-developed turbulent fluid flow in a channel was performed in a box with dimensions of $1900\nu/v^*$ in the streamwise direction (x_1), $300\nu/v^*$ in the wall-normal direction (x_2), and $950\nu/v^*$ in the spanwise direction (x_3), where ν is the kinematic viscosity. A pseudospectral fractional step method (Lyons et al., 1991) was used for the spatiotemporal discretization. The computational grid was $128 \times 65 \times 128$. The resolutions in the streamwise and spanwise directions were $\Delta x_1^+ = 15$ and $\Delta x_3^+ = 7.4$, where the superscript plus represents the variable was made dimensionless with the wall parameters, v^* and ν. The resolutions in the perpendicular direction varied from $\Delta x_2^+ = 0.18$ at the wall to $\Delta x_2^+ = 7.4$ at the channel center. No slip boundary conditions were used at $x_2 = \pm H$ and periodicity was assumed in the x_1 and x_3 directions. The time step was $\Delta t^+ = 0.25$. The gas velocity seen by the particles was calculated using a mixed spectral-polynomial interpolation scheme developed by Kontomaris et al. (1992). At time zero, the particles were distributed uniformly on each wall.

4. Stochastic simulation

4.1. A modified Langevin equation

A modified Langevin equation is formulated for a fluctuating component of fluid velocity, u_i, normalized by the Eulerian root-mean-square value of the velocity fluctuation, σ_i (Thomson, 1984). The change of the fluid velocity seen by a solid particle, $\mathrm{d}u_i$, over a time interval $\mathrm{d}t$ is given by

$$\mathrm{d}\left(\frac{u_i}{\sigma_i}\right) = -\frac{u_i}{\sigma_i \tau_i}\mathrm{d}t + \overline{\mathrm{d}\mu_i} + \mathrm{d}\mu_i', \tag{6}$$

where τ_i is the Lagrangian time scale and $\mathrm{d}\mu_i$ is a random forcing function which consists of a mean drift $\overline{\mathrm{d}\mu_i}$ and a fluctuation $\mathrm{d}\mu_i'$. The fluid velocity, U_i, is defined as the sum of the Eulerian average, $\overline{U}_i(x_2)$, and u_i calculated from Eq. (6). The specification of τ_i is discussed in the next section. The mean drift $\overline{\mathrm{d}\mu_i}$ is obtained by relating $\mathrm{d}(u_i/\sigma_i)$ to the substantial Eulerian derivative and taking an ensemble average of Eq. (6) (Iliopoulos and Hanratty, 1999):

$$\overline{\mathrm{d}\mu_i} = \frac{\partial\left(\frac{\overline{u_2 u_i}}{\sigma_i}\right)}{\partial x_2}\mathrm{d}t, \tag{7}$$

where an overbar indicates an ensemble average. The use of Eq. (7) to counterbalance the mean drift velocity associated with inhomogeneous turbulence is discussed by Legg and Raupach (1982) and Thomson (1984). The Eulerian averages given by the DNS are used to obtain the ensemble averages and σ_i. The covariances of $\mathrm{d}\mu_i'$ are obtained by using the definition of a stochastic differential (Iliopoulos and Hanratty, 1999),

$$\overline{\mathrm{d}\mu_i' \mathrm{d}\mu_j'} = \left\{ \frac{\partial\left(\frac{\overline{u_i u_j u_2}}{\sigma_i \sigma_j}\right)}{\partial x_2} + \frac{\overline{u_i u_j}}{\sigma_i \sigma_j}\left(\frac{1}{\tau_i} + \frac{1}{\tau_j}\right) \right\} \mathrm{d}t + o(\mathrm{d}t)^2. \tag{8}$$

The random forcing function $\mathrm{d}\mu_i'$ is assumed to be jointly Gaussian (Mito and Hanratty, 2002). Thus the triple correlations in Eq. (8) are taken to be zero because of the assumption of Gaussian turbulence. The condition of well-mixedness (Thomson, 1987) for the system constructed with Eqs. (6)–(8) was verified in the calculation of dispersions of fluid particles from uniformly distributed sources (Mito and Hanratty, 2002).

4.2. Selection of the time constants τ_i

A critical issue in using a modified Langevin equation is the specification of the time constants, τ_i. For fluid particles they have been defined by the scaling law (Monin and Yaglom, 1975; Tennekes, 1979)

$$\tau_i = \frac{2\sigma_i^2}{C_0 \tilde{\varepsilon}}. \tag{9}$$

Here $\tilde{\varepsilon}$ is a modified dissipation rate of turbulent energy defined as

$$\tilde{\varepsilon} = \nu \left\{ \overline{\frac{\partial u_i}{\partial x_j}\frac{\partial u_i}{\partial x_j}} - 2\left(\frac{\partial \sqrt{k}}{\partial x_j}\right)^2 \right\}, \tag{10}$$

where k is the turbulent energy and $\tilde{\varepsilon}$ excludes large contributions close to a wall in a region where the velocity profiles are linear and oscillating with time (Jones and Launder, 1972). Sawford (1991) suggested $C_0 = 7$ and Du et al. (1995) suggested $C_0 = 3 \pm 0.5$ from experiments in a homogeneous, isotropic field. Mito and Hanratty (2002) obtained $C_0 = 3.5$ from experiments done in a DNS of fully-developed turbulent flow in a channel. Mito and Hanratty (2002) found that this scaling law is a good approximation but that it does not capture the correct behavior in the near-wall region ($x_2^+ < 100$).

In the modeling of the fluid velocities seen by solid particles, Perkins (1992) and Pozorski and Minier (1998) suggested that the time constants should be adjusted to account for the inability of solid particles to follow exactly fluid particles. Iliopoulos et al. (2003) changed the functions describing the time constants and found the simple approach of using the values characterizing dispersion of fluid particles to be adequate. In separate calculations, we came to the same conclusion as Iliopoulos et al. (2003) (for the conditions considered in this paper).

5. Numerical method

5.1. Time advancement scheme for the particle tracking

At each time step, the displacements of the particles, defined by Eq. (3), are calculated by using a second-order Adams–Bashforth method. When using the DNS, the fluid velocities seen by particles are calculated by interpolating the velocities obtained from the DNS after the time step that has just been completed. In the stochastic simulation, Eq. (6) is solved by using a fully implicit method in order to specify the fluid velocity. The same time step that is used in the DNS, $\Delta t^+ = 0.25$, is assumed for solving Eq. (6). The velocities of the solid particles are calculated with Eq. (4) by using a second-order Adams–Bashforth method. At the initial time step, a first-order Euler explicit method was used to calculate the displacements and the velocities of particles. Particles are removed from the field when they are at a distance of $d_p/2$ from a wall.

5.2. Calculation of fully-developed fields

Fully-developed stationary concentration fields are calculated by using a Lagrangian method, which pictures the field as resulting from instantaneous wall sources that propelled solid particles into the field at different previous times. For the flow model shown in Fig. 1, this calculation becomes simple since the concentration and other statistics are varying only in the x_2-direction.

The computational experiment involved the injection of N_b ($=10{,}000$) particles from the bottom wall at time zero. The number of particles whose centers are in bins of size Δx_2, $n_b(x_2, t)$, was calculated at different times ($t > 0$). The ratio n_b/N_b, obtained in these calculations, represents the probability of the particles being in the bin at x_2 at time t, $P_b(x_2, t)\Delta x_2$, where $P_b(x_2, t)$ is the probability density function. Now N_b ($= R_{Ab} A \Delta t$) represents the strength of a wall source, where

Δt is a time interval over which N_b drops are admitted from a wall source and A is the area of the wall over which the drops are charged. Thus, for a given wall source

$$n_b(x_2,t) = (R_{Ab}A\Delta t)P_b(x_2,t)\Delta x_2. \tag{11}$$

Define the concentration determined at x_2, t for the wall source as $C_{bw}(x_2,t) = n_b(x_2,t)/A\Delta x_2$. Thus

$$\frac{C_{bw}(x_2,t)}{R_{Ab}} = \Delta t P_b(x_2,t) \tag{12}$$

is the contribution to the fully-developed concentration at x_2 for particles that were admitted to the field for times between $t-\Delta t$ and t. At a given x_2 the particle concentration for the fully-developed field, $C_b(x_2)$, represents contributions from sources that were admitted at all previous times, $-\infty < t < 0$, so that $C_b(x_2)$ is approximated as the integral of results for single wall sources, $C_{bw}(x_2,t)$, from $t=0$ to $t=\infty$ (Hanratty, 1956; Papavassiliou and Hanratty, 1997):

$$\frac{C_b(x_2)v^*}{R_{Ab}} = v^*\int_0^\infty \mathrm{d}t P_b(x_2,t). \tag{13}$$

The dimensionless contribution from sources located at the top wall is

$$\frac{C_t(x_2)v^*}{R_{At}} = v^*\int_0^\infty \mathrm{d}t P_t(x_2,t). \tag{14}$$

Thus, a dimensionless concentration in the fully-developed field, $Cv^*/R_{Ab}(x_2)$, is calculated from

$$\frac{Cv^*}{R_{Ab}} = \frac{C_b v^*}{R_{Ab}} + \frac{R_{At}}{R_{Ab}}\frac{C_t v^*}{R_{At}}, \tag{15}$$

where $C = C_b + C_t$ and Eq. (2) is used to specify the relative strengths of the top wall sources. Other statistics in the fully-developed field, which may include velocity components, are calculated with the average values taken for the contributions from sources on the bottom and top walls, f_b and f_t, as

$$f = \frac{C_b f_b + C_t f_t}{C}. \tag{16}$$

6. Results

6.1. Parameters representing the calculations

The motion of a sphere described by Eqs. (4) and (5) is governed by the particle diameter, d_p, the density ratio, ρ_p/ρ_f, and the Froude number, $Fr\ (= v^{*2}/2gH)$. The dimensionless inertial time constant of the particles is defined as

$$\tau_p^+ = \frac{4d_p^+(\rho_p/\rho_f)}{3C_D|\boldsymbol{V}^+ - \boldsymbol{U}^+|} \tag{17}$$

and the free-fall velocity was obtained from Eq. (4) as

$$V_T^+ = \tau_p^+ g^+. \tag{18}$$

The conditions, $d_p^+ = 0.368$, $Fr = 0.6$, $\rho_p/\rho_f = 2650$, were chosen so as to have a dimensionless inertial time constant of $\tau_p^+ \cong 20$ and $V_T^+ = 0.11$. The dimensionless gravitational constant g^+ $(= 1/2FrRe_\tau)$ was set at 5.6×10^{-3}.

6.2. Single wall sources

Fig. 2 shows probability density functions, P_b, (concentration fields) of particles that originate from a single source on the bottom wall. The ordinate is made dimensionless by using the viscous length (v/v^*). The abscissa is the dimensionless distance from the bottom wall. The concentration fields were calculated by using first-order weights for each particle that are defined with the distances between the center of the particle and the edges of the bins between which the particle exists. This method increases accuracy of sampling compared with a zeroth-order method that uses a single weight for each particle in a sampling bin. The centers of the 129 sampling bins are distributed from $x_2 = d_p/2$ to $x_2 = 2H - d_p/2$ by using a cosine function, which gives bin sizes of $\Delta x_2^+ = 0.02$ at $x_2 = d_p/2$ and of $\Delta x_2^+ = 3.7$ at the center of the channel. The temporal variations of the concentration fields through $t^+ = 250$ are presented. The area under a curve is the fraction

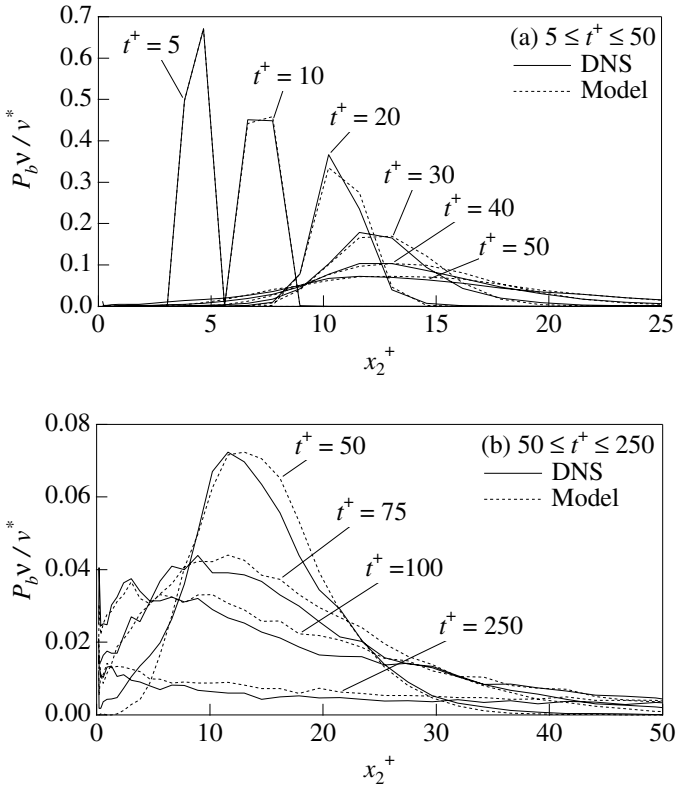

Fig. 2. Distributions of particles from a wall source located on the bottom wall.

of the particles which remain in the flow at the specified t^+. The solid and dotted curves, respectively, present calculations in which fluid velocities seen by particles are obtained from a DNS and from the stochastic analysis (the model). Good agreements are noted. At small times, $t^+ < 40$, peaks are observed to move away from the wall because of the inertia of particles injected with $V_2^{0+} = 1$ at $x_2^+ = d_p^+/2$, $t^+ = 0$. The peak reaches $x_2^+ = 13$ at $t^+ = 40$. At $t^+ = 70$ it starts moving toward the bottom wall because of gravitational effects. These results suggest that the particles tend to lose memory of their initial motion at $x_2^+ \cong 0.65 V_2^{0+}\tau_p^+$, where $V_2^{0+}\tau_p^+$ is the stopping distance in a motionless fluid. As time proceeds the particles are mixed by the fluid turbulence and gravitational settling.

It is noted that at $t^+ \geqslant 50$ the concentration is skewed in the direction of positive x_2^+. This skewness is larger for the model. A consequence of this is that the particles reach the wall slightly sooner when calculations are done with the DNS. At larger t^+ the peak disappears and the maximum exists close to the wall. However, again, the model predicts slightly smaller concentrations near the wall and slightly larger concentrations at larger x_2^+. Similar results were observed in a study of dispersion of solid particles from a point source located at $x_2^+ = 40$, except that the peak at small t^+ was at the injection location (Iliopoulos et al., 2003). Calculations with a modified Langevin equation, in which skewness of the fluid velocity fluctuations was considered, were carried out. These showed no improvement. The differences, therefore, appears to reflect limitations in the model.

Fig. 3 presents temporally varying concentration fields of particles from a single source on the top wall. The definitions of the axes are the same as for those in the Fig. 2. Peaks are observed to keep moving downward due to the influence of gravitational settling. Good agreement is noted between the calculations with the model and the experiments in the DNS. However, the model predicts slightly smaller dispersion (larger concentrations) near the peaks at $t^+ \geqslant 75$.

The number of the particles, n, which entered the flow field from sources on the bottom and top walls at time zero and remain at time t^+ was calculated. Fig. 4 presents the time derivatives with a minus sign, $-\mathrm{d}n/\mathrm{d}t^+$, that is, the rates of deposition. Particle deposition starts on the bottom wall at $t^+ = 35$ in the DNS and at $t^+ = 60$ in the model simulation, consistent with the concentration profiles shown in Fig. 2. The rate of deposition is larger for the DNS than for the model simulation at small times $t^+ < 250$ and it becomes almost the same after this time period. This rate is strongly affected by the concentration of particles near the wall. The times at which the peaks are observed in Fig. 4 correspond to the times at which the concentrations at the wall assume maximum values. These times are the same for the model and for the DNS. All the particles deposit by $t^+ = 7900$ for the DNS and by $t^+ = 14{,}300$ for the model simulation.

6.3. Fully-developed concentration fields

The ratio of the rate of atomization at the top wall to that at the bottom wall, R_{At}/R_{Ab}, was calculated as 3.6×10^{-3} by using Eq. (2) for the DNS and as 3.9×10^{-3} for the model simulation. Fig. 5 shows dimensionless concentration profiles in the fully-developed field that were calculated from the data for wall sources on the bottom and top walls by using Eqs. (13) and (14). The model simulation approximately captures the concentration field which was calculated by using the DNS. However, it predicts larger concentrations throughout the domain. This reflects the cumulative effect of underpredicting the rate of deposition for $t^+ \leqslant 200$, shown in Figs. 2 and 4.

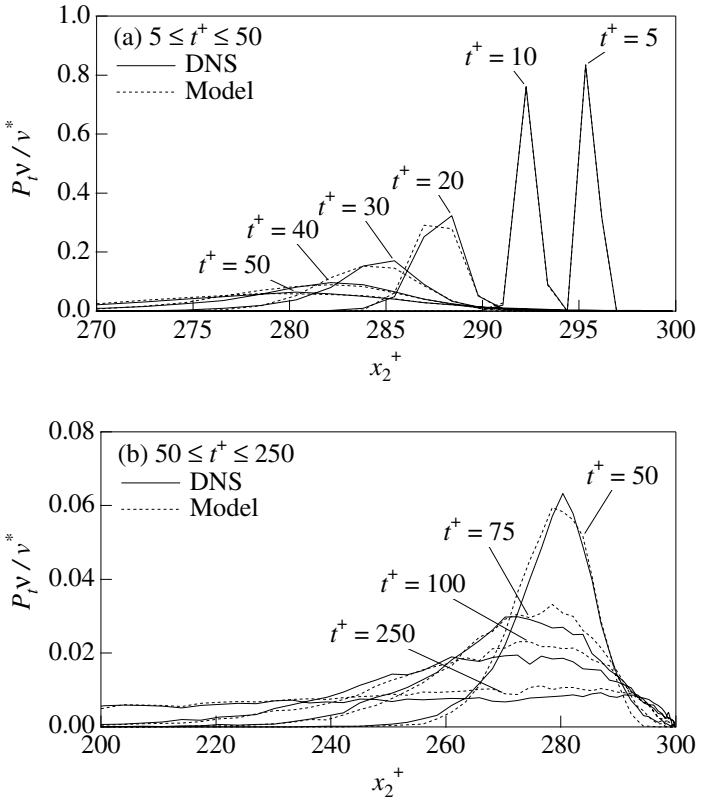

Fig. 3. Distributions of particles from a wall source located on the top wall.

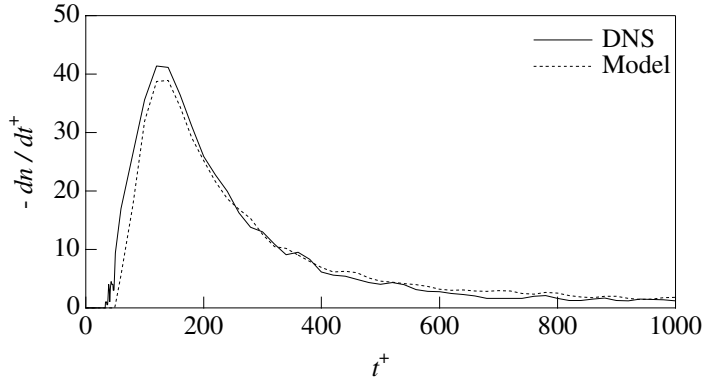

Fig. 4. The rate of decrease of particles remaining in the field.

Lines with dots and dashes are solutions of a diffusion model described with the equation

$$-\varepsilon_t \frac{dC}{dx_2} - V_T C = a, \tag{19}$$

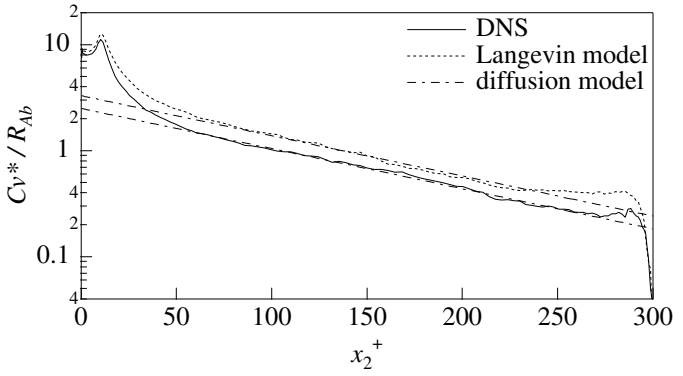

Fig. 5. Distributions of particles in the fully-developed field.

where a is the flux (equal to $\overline{V_2}C$) and ε_t is a turbulent diffusivity (Paras and Karaberas, 1991; Pan and Hanratty, 2002). In a fully-developed field, $a = 0$ and a solution of Eq. (19) becomes exponential when a constant value is assumed for the turbulent diffusivity. (This approximation is expected to be valid only in the central region of the channel.) The turbulent diffusivities calculated from the concentration profiles for the DNS and the model simulation are very close. Thus $\varepsilon_t^+ = 12.5$ ($\varepsilon_t/v^*H = 0.083$) is assumed for both of the lines shown in Fig. 5. It is observed that the turbulent diffusivity model gives a good approximation for both calculations in the central regions of the channel. Thus, turbulent dispersion for the fully-developed field is captured quite well in the model simulation.

The peaks in the fully-developed concentration profiles reflect the initial mixing process. Fig. 6 presents filtered concentration profiles of the fully-developed fields for which only particles that have existed in the field over certain times are taken into account. The profiles for $t^+ > 0$ correspond to the fully-developed concentration fields shown in Fig. 5. For both the DNS and the model simulation, it is observed that the peaks in the near-wall region are caused by the particles that entered the field at recent times, $t^+ \leqslant 50$–75. The distance of the peaks from the wall approximately corresponds to the stopping distance of the injected particles that is observed in Fig. 2. After an initial mixing process at $0 < t^+ \leqslant 50$–75, deposition starts. A large fraction of the particles close to the wall is observed to be contributed by sources that have been in the field for times less than 200 wall units. It is noted that the filtered profiles show slightly larger Cv^*/R_{Ab} for the model.

Since R_{Ab} equals the rate of deposition R_{Db} one can replace R_{Ab}/C with R_{Db}/C in Fig. 5. The particles that are observed at the wall ($x_2^+ = d_p^+/2$) can be divided into two populations for the free-fall velocity that is considered ($V_T^+ = 0.11$). One, with concentration $C_{W+} = R_{Ab}/V_2^0$, has the velocity V_2^0 with which the particles are injected. The other, with concentration $C_{W-} = -R_{Db}/\overline{V}_W$, has an average negative velocity $\overline{V}_W$ and contains all of the depositing particles. From algebraic considerations which recognize that both populations contribute to the concentration at the wall, C_W ($= C_{W+} + C_{W-}$), one can show that

$$\frac{C_W v^*}{R_{Ab}} = \frac{1}{V_2^{0+}} - \frac{1}{\overline{V}_W^+}. \tag{20}$$

The slightly larger value of $C_W v^*/R_{Ab}$ obtained with the stochastic model (Figs. 5 and 6), therefore, suggests that the model is predicting slightly smaller values of $-\overline{V}_W$. For the case considered in this paper ($V_T^+ = 0.11$) all of the particles in the C_{W-} population have negative velocities. However, this is not the situation for $V_T^+ = 0$. Then, a large number of particles with very small positive or negative velocities are trapped in a region very close to the wall.

For $V_T^+ = 0.11$, C_{W-} and $\overline{V}_W$ can be calculated by conditionally sampling particles with negative velocities in the bin next to the wall. Fig. 7 presents probability density functions of $-V_W$ obtained in this way. They were calculated by using a first-order sampling method and 65 bins distributed from $V_W^+ = 0$ through $V_W^+ = -2$ with a hyperbolic tangent function which gives bin sizes of $\Delta V_W^+ = 1.7 \times 10^{-5}$ at $V_W^+ = 0$ and $\Delta V_W^+ = 7.7 \times 10^{-2}$ at $V_W^+ = -2$. The line with dots and dashes represents the free-fall velocity, $-V_T^+ = 0.11$. Peaks are located approximately at $-V_T^+$. Thus, it can be seen that the free-fall velocity has a large effect on the deposition process. The long tails in the region of large $-V_W^+$ show contributions from particles which start a free-flight at some distance from the wall. Good agreement is noted between calculations done with the DNS and with the stochastic model. However, the model slightly underestimates the fraction depositing with $-V_W^+ > 0.2$. The mean velocity, $-\overline{V}_W^+$, is calculated from the pdf profiles as −0.133 for the DNS and −0.125 for the model simulation. This difference is largely caused by differences

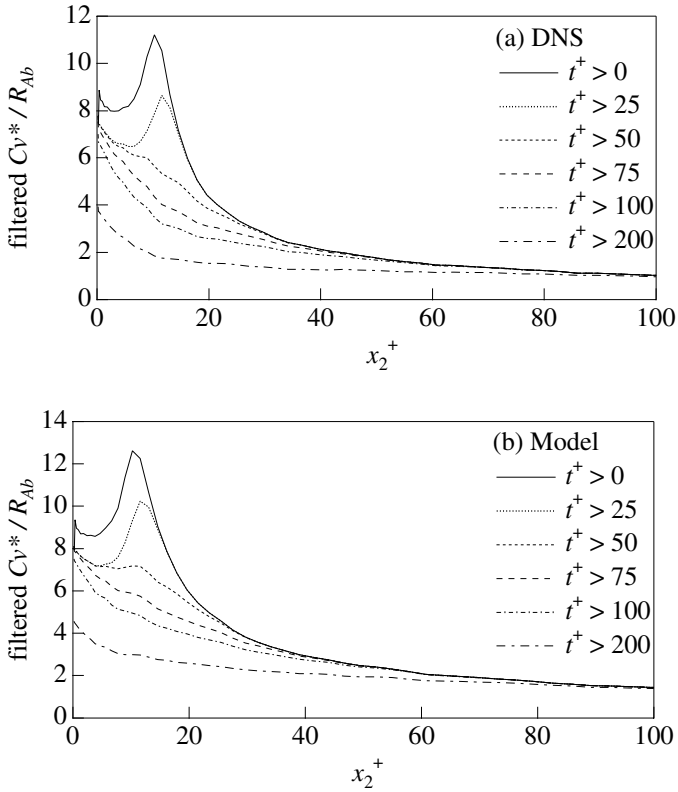

Fig. 6. Filtered concentration fields.

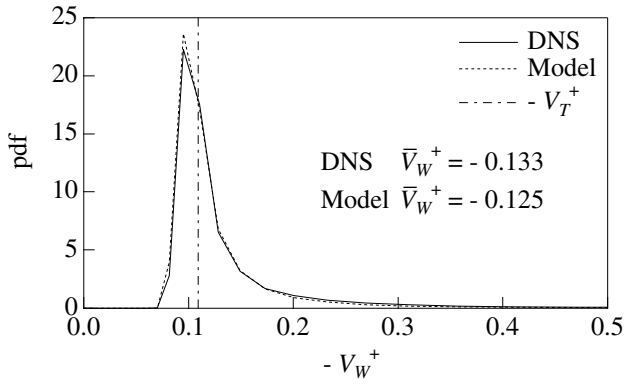

Fig. 7. Probability density functions of wall-normal velocities of particles at the bottom wall.

observed in the velocities of the particles that contribute to the tails. The fractions of the particles in these tails are very small but their contributions to the deposition fluxes are not small. For example, the fractions representing the contributions of the tails for $-V_W^+ \geqslant 0.2$ are 20% for the DNS and 13% for the model.

6.4. Spatial variations of particle velocities

Fig. 8 presents streamwise mean velocities of the particles in the fully-developed field. The curve with dots and dashes represents the mean velocity of the fluid. Good agreement between the DNS and the model simulation is noted. The streamwise mean velocity of the particles becomes larger than the fluid mean velocity in the near-wall region because of the assumption of a large x_1 component of the injection velocity, $V_1^+ = 15$, and the contribution of the free-flight particles which reached this region without completely losing the large streamwise velocities at the origin of the free-flight. By considering an imaginary source at $x_2^+ \cong 11$, which corresponds to the locations of the peaks in the concentration fields shown in Fig. 5, the increased mean velocities below this

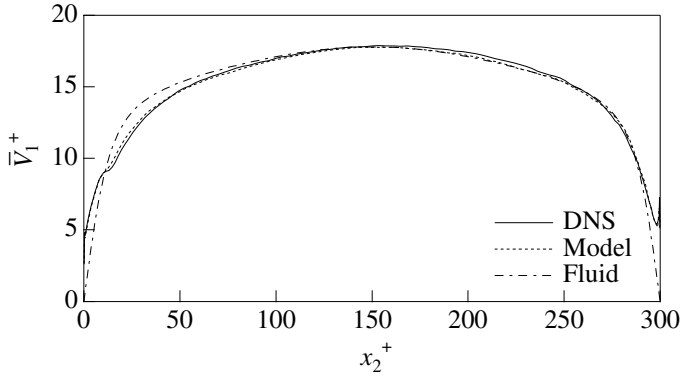

Fig. 8. Streamwise mean velocities of particles in the fully-developed field.

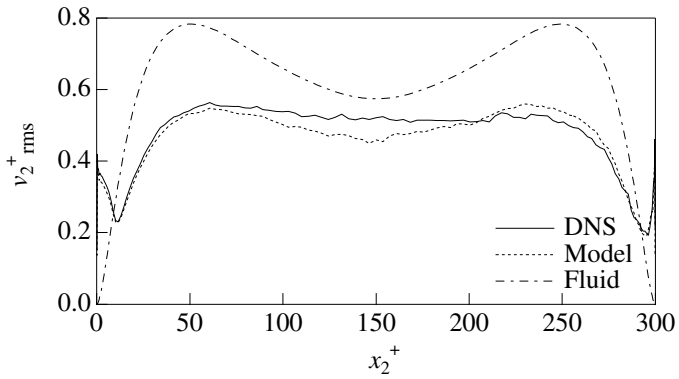

Fig. 9. Root-mean-square values of the wall-normal fluctuating component of particle velocity in the fully-developed.

point and decreased mean velocities above this point are understood. The wall-normal mean velocities of the particles in the fully-developed field are zero at all locations for the DNS and the model simulation. This result is consistent with the existence of a stationary field.

Fig. 9 presents root-mean-square values of the wall-normal fluctuating component of the particle velocity in the fully-developed field. The curve with dots and dashes represents the Eulerian wall-normal fluid turbulence. Because of particle inertia, the particle turbulence is smaller than the fluid turbulence except in the near-wall region, where it is larger because of the large velocity contributions by entrainment and by depositing particles in free-flight (Iliopoulos et al., 2003). The model and the DNS are in good agreement. The model, however, slightly underestimates the particle turbulence in the center region of the channel. The value of $v_{2\,\mathrm{rms}}^{+}$ at the wall (equal to 0.42 for the DNS and 0.40 for the model) is associated mainly with the velocity of the injected particles. The decrease with increasing x_2 reflects a slowing of the injected particles due to fluid resistance. The minimum corresponds to the location of the maxima in the concentration (Fig. 6) where the injected particles appear to be completely mixed.

Fig. 10 presents probability density functions of the particle velocities at $x_2^+ = 1$, 5 and 13 in the fully-developed field. The areas under the curves are unity. In the vicinity of the wall $x_2^+ < 7$, two

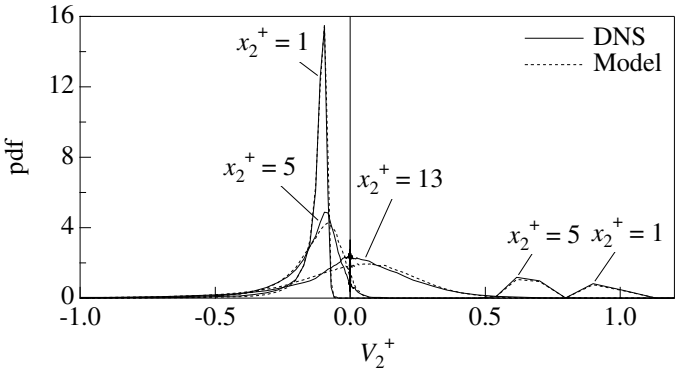

Fig. 10. Velocity distributions of particles located at distances above the bottom wall in the fully-developed field.

separate distributions are observed. One, in the positive region, represents particles injected into the flow at $x_2^+ = d_p^+/2$ with a velocity $V_2^+ = 1$. The other one shows velocities associated with the deposition process. At $x_2^+ = 13$ the injected particles are mixed with the other particles and the distribution has a single peak. The influence of the free-fall velocity is evident only for $x_2^+ \leqslant 5$. Good agreements between the DNS and the model simulation are noted.

6.5. Dimensionless rate constants

A dimensionless rate constant (McCoy and Hanratty, 1977) can be defined as

$$k_{DB}^+ = \frac{R_{Ab} + R_{At}}{2C_B v^*}, \tag{21}$$

where C_B is the mean concentration of the fully-developed field defined as

$$C_B = \int_0^2 C \, d\left(\frac{x_2}{H}\right). \tag{22}$$

The bulk rate constant, k_{DB}^+, is 0.37 for the DNS and 0.29 for the model simulation. The model simulation underestimates the rate constant because of the underestimation of $-\overline{V}_W$ and the overestimation of particle diffusivity for $x_2^+ < 50$. Eq. (21) represents an average of the rates of the deposition on the bottom and top walls. These rates can be separately defined by using concentrations at a specified distance from the walls. If the concentrations at $x_2^+ = 40$ from the walls are chosen, the rate constants for the bottom and top walls are, respectively, defined as

$$k_{Db40}^+ = \frac{R_{Ab}}{C_{b40} v^*}, \tag{23}$$

$$k_{Dt40}^+ = \frac{R_{At}}{C_{t40} v^*}, \tag{24}$$

where C_{b40} and C_{t40} represent the concentrations at a distance of $x_2^+ = 40$ from the bottom and top walls. The rate constants for the bottom wall, where gravity is aiding deposition, are calculated from Eq. (23) as 0.47 for the DNS and 0.34 for the model simulation. The rate constants for the top wall, where gravity is hindering deposition, are calculated with Eq. (24) as 0.014 for the DNS and as 0.0095 for the model simulation.

The dispersion process occurs approximately in two steps. At small times particles from the wall sources mix with the fluid and no deposition occurs. The filtered curves, shown in Fig. 6, for $t^+ > 50$ are more representative of the concentration field associated with deposition than is the profile in Fig. 5. It is of interest to note that the filtered concentration at $x_2^+ = 40$ is the same for $t^+ > 0$ and for $t^+ > 50$. The definition of rate constants in terms of C_{b40} therefore, appears to be a sounder choice since it is less sensitive to the details of the original mixing process.

7. Interpretation of the concentration profiles

A physical interpretation of the concentration profile shown in Fig. 5 is a challenging task. It might be useful to consider the mean transport velocity of the particles as the result of

contributions from diffusion, V_d, gravity, V_g, turbophoresis, V_{tp}, free-flight to the wall, V_{ff}, and the mixing motion associated with the injection of the particles at the wall, V_i:

$$\overline{V} = V_d + V_g + V_{tp} + V_{ff} + V_i, \tag{25}$$

where $\overline{V} = 0$ for a fully-developed field. The turbophoretic flux results from a gradient in the turbulence (Caporaloni et al., 1975; Reeks, 1983; Brooke et al., 1994).

$$V_{tp} = -\tau_p \frac{d\overline{v_2^2}}{dx_2}. \tag{26}$$

If the particles have been in the field long enough they will, on average, reach a terminal velocity so that $V_g = -V_T$.

Particles arrive at the wall by gravitational settling and by turbulence through a free-flight mechanism. The particles lag behind the fluid velocity fluctuations. As they approach the wall they "disengage" from the fluid turbulence. If they have a large enough velocity they move into a region of lower fluid turbulence and glide to the wall by free-flight or by gravitational settling. This process has been described in detail by Brooke et al. (1994).

In the center regions of the channel the two important fluxes are V_g and V_d so the concentration field is defined by Eq. (19). If ε_t is constant one calculates that the concentration decreases exponentially with x_2. Since the turbulent diffusivity decreases at small x_2 a departure from the exponential relation and increases in the magnitude of dC/dx_2 are observed as x_2 decreases.

The turbophoretic velocity is important for $x_2^+ < 60$ or for $x_2^+ > 240$. The gradients of turbulence in these regions are such that they cause particle drift toward the two walls. At the bottom wall this will enhance the influence of gravity. For $V_T = 0$ it is the dominant mechanism for bringing particles into the wall region (Brooke et al., 1994).

For the cases in which there is no top wall one would expect the exponential relation to extend out to very large x_2. However, for the case of a channel flow, turbophoresis can greatly alter the behavior. The influence is different from what is observed at the bottom wall in that it opposes the influence of gravity. A balance equation can be written as

$$\varepsilon_t \frac{dC}{dx_2} = -V_T C - \tau_p \frac{d\overline{v_2^2}}{dx_2} C. \tag{27}$$

The turbophoretic effect starts to have an influence at $x_2^+ \cong 230$. There is a region where the turbophoretic and the gravity effects approximately balance and, from Eq. (27), the concentration gradient is small (see Fig. 5). As already shown in Fig. 7, particles are thrown to, or close to, the bottom wall by a free-flight mechanism. Particles that stop short are carried to the wall by gravity. At the top wall, gravity carries particles away from the boundary. Thus, there is a sharp decrease in particle concentration at the wall as $x_2^+ \to 300$. Only particles with very large turbulent velocities reach the wall.

The calculation of concentration profiles with Eq. (25) is not clearcut because of uncertainties in representing V_i and V_{ff} and of inaccuracies in assuming $V_g = -V_T$. As shown in Fig. 6 the influence of the injection process on the concentration profiles is associated mainly with sources that have been in the field for small times. The filtered concentration field for $t^+ > 75$, partially shown in Fig. 6, is presented in Fig. 11 for $0 \leqslant x_2^+ \leqslant 300$ as a solid line. This should be more representative

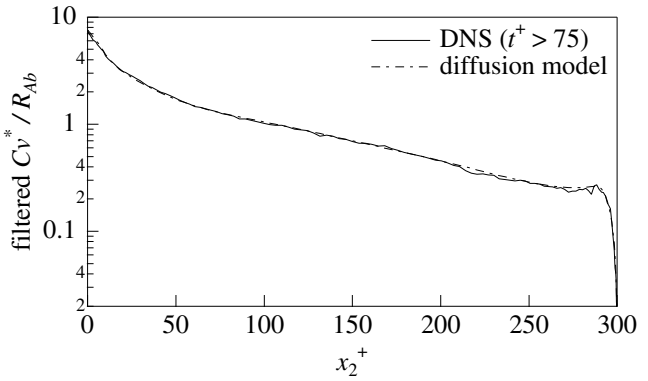

Fig. 11. Solution of a diffusion model for a filtered concentration field.

of the deposition process. The dashed line in Fig. 11 represents a calculation with $C_W v^*/R_{Ab} = 7.8$ which used Eq. (25) with $V_i = 0$ and adjusted the spatial variation of ε_t so as to obtain a good fit. The turbophoretic velocity, V_{tp}, was calculated from Eq. (26). The approximation was made that the use of $\overline{v_2^2}$ obtained for the filtered field would take account of the contributions from V_{ff} and from errors in assuming $V_g = -V_T$. Fig. 12 presents values of $(\overline{v_2^2})^{1/2}$ for the filtered field for $t^+ > 75$. It does not change from the value for the unfiltered field at $50 < x_2^+ < 250$. The main difference is that a minimum does not exist close to the bottom wall and the value at the wall is largely associated with depositing particles. (It is 0.15 for the DNS and 0.14 for the model.) The influence of filtering on $\overline{v_2^2}$ at the top wall is not understood. However, it should be pointed out that the number of particles at the top wall is very small (see Fig. 11). Mean fluxes, calculated for the filtered fields, are given in Fig. 13. It is noted that $\overline{V}$, in Eq. (25), is not zero since the contribution from the initial mixing process, V_i, is ignored.

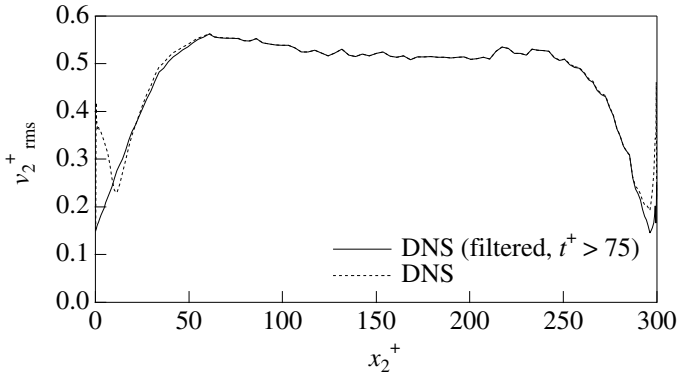

Fig. 12. Filtered root-mean-square of wall-normal particle velocity component in which contributions from the particles in the initial mixing process through $t^+ = 75$ are ignored.

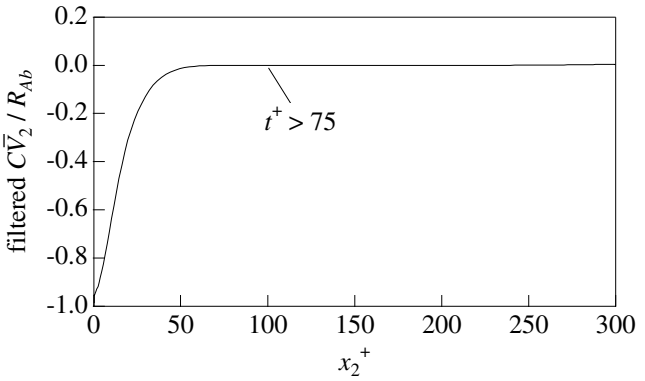

Fig. 13. Filtered wall-normal mean flux in which contributions from the particles in the initial mixing process through $t^+ = 75$ are ignored.

8. Discussion and conclusions

8.1. Principal contributions

The two principal contributions of this paper are the evaluation of a stochastic method (that uses the Langevin equation to represent fluid turbulence) to describe the behavior of a wall source of solid spheres and the use of these results to enhance our physical understanding of the dispersion and deposition processes.

8.2. Testing the stochastic analysis

Considering the complexity of the turbulence close to a wall and the simplicity of the model it is satisfying (and surprising) that the agreement with experiments done in a DNS is so good. Furthermore, the calculation required the use of only about 3% of the CPU time and memory that were needed in the DNS experiments. These results have encouraged us to use the model at a higher Reynolds number (for which the advantage would be much greater) and for a wide range of conditions in order to obtain a physical understanding of the influence of gravitational settling and of particle inertia on the rate of deposition under conditions analogous to what is found in gas–liquid annular flow. The results of these studies are presented in Part 2 of this paper.

8.3. Behavior of a wall source (from DNS results)

A simple model for a wall source is used whereby solid spheres are ejected from the wall at a constant velocity, $\boldsymbol{V}^0$. The behavior is similar to what has been observed for particles that are admitted to the flow at a distance from the wall, x_2, whose value depends on the magnitude of V_2^0.

The dispersion of particles originating from a wall source occurs approximately in two stages. For $t^+ < 75$ the injected particles are entrained in the turbulent flow and a peak in the concentration appears. For $t^+ > 75$ the concentration field has a maximum value close to the wall and deposition causes decreases in the number of particles in the field. At large enough times all the

particles deposit. The particles first reach the wall at $t^+ \cong 35$. Their concentration at the wall increases and eventually reaches a maximum at $t^+ \cong 100$. At time $t^+ \cong 120$ only 20% of the particles have deposited.

8.4. Wall transfer (from DNS results)

Concentration profiles associated with wall transfer can be represented as the sum of particles that have originated from sources that entered the field at previous times of $0 < t^+ < 7900$. The peak that is observed at $x_2^+ = 11$ is caused by peaks observed at small times in the calculations for a wall source.

This is illustrated in Fig. 6 where filtered concentration profiles are presented. By considering only point sources that have been operating for $t^+ > 75$, no evidence of the injection process is observed. The concentration decreases monotonically with x_2^+ and the concentration profile is the same for the filtered and unfiltered data for $x_2^+ > 40$. The dimensionless concentration of particles with a negative wall-normal velocity component at the wall, given as $C_{W-}v^*/R_{Ab}$, is 7.8 for the filtered profile (for $t^+ > 75$). The magnitude of the average velocity of these particles, $-\overline{V}_W$, is calculated, as $0.13v^*$ either from the measured particle velocity distribution at the wall (Fig. 7) or from the value of $R_{Ab}/C_{W-}v^*$ by using Eq. (20).

For the conditions considered ($V_T^+ = 0.11, \tau_p^+ = 20$) gravity is having a strong effect on the distribution of the particles (so that the ratio R_{At}/R_{Ab} is only 3.6×10^{-3}) and on the rate constants characterizing deposition at the two walls. This is also evident in the probability distribution of the velocities of particles (Fig. 7). Most (92%) of the particles have a velocity close to the settling velocity ($0 < -V_W^+ \leqslant 0.2$). However, these contribute 80% of the deposition flux. The rest of deposition flux is associated with particles in the tail of the distribution. For example, the 3% of the particles which have velocities ($-V_W^+$) greater than 0.3 make a contribution of 10% to the deposition flux.

Many of the depositing particles have velocities much greater than the settling velocity and the turbulent fluid velocities close to the wall. As pointed out by Brooke et al. (1994), these large velocity particles arrive by "free-flight" from regions that are distant from the wall. If the channel is vertical many of these particles stop before they reach the wall and accumulate in the viscous sublayer. This does not happen for the case considered since gravity carries the particles to the wall and, therefore, enhances deposition.

The particle flux at any location is the product of the average velocity, $\overline{V}_2$, and the concentration, C. The velocity can have contributions from gravitational settling, turbulent diffusion (due to concentration gradients), turbophoresis (due to gradients in turbulence), velocities associated with the injection of particles at the wall, free-flight motions to the wall. The understanding and definition of these different contributions will require studies over a large range of V_T^+ and τ_p^+. For the conditions considered in this paper, the concentration field in the center of the channel would have small contributions from injection velocities, free-flight and turbophoresis. Turbulent diffusion is balanced by gravitational settling. Thus the integration of Eq. (19) for a constant ε_t and for $a = 0$ gives

$$\ln\frac{C}{C_R} = -\frac{V_T}{\varepsilon_t}(x_2 - x_{2R}), \tag{28}$$

where C_R is the concentration at a reference location. If $\varepsilon_t = \xi v^* H$

$$\ln \frac{C}{C_R} = -\frac{V_T}{\xi v^*} \frac{x_2 - x_{2R}}{H}. \tag{29}$$

This result provides a rough fit for the data in the center of the channel and suggests that the asymmetry of the profile increases with increasing V_T/v^* (Baik and Hanratty, 2003).

The fit to the data can be extended to smaller x_2 by allowing ε_t, in Eq. (19), to change with x_2 and by considering turbophoresis effects, as shown in Fig. 11.

8.5. Errors in the stochastic analysis

The stochastic analysis captures all of the physics of the deposition and mixing processes. However small, but significant, discrepancies need to be pointed out.

One is the average of the negative velocities of the particles in the bin closest to the wall. As has already been mentioned, the intercept of Cv^*/R_{Ab} in the filtered profile for $t^+ > 75$ (in Fig. 6) gives $\overline{V}_W = -0.133v^*$ for the calculations with the DNS. The model gives a higher Cv^*/R_{Ab} and $\overline{V}_W = -0.125v^*$. A possible explanation is given in Fig. 7, which presents the probability density function of the velocities of the particles in the bin closest to the wall. Slightly larger values in the tail are observed for calculations done with the DNS. These small differences in the free-flight contributions can cause differences in the average velocity of the particles very close to the wall.

The most noticeable discrepancy is in the calculation of the concentration profile, shown in Fig. 5, where the DNS is seen to predict lower concentrations. This is partly caused by the prediction of lower $-\overline{V}_W$ by the model. This can be taken into account partially by plotting C/C_W. A difference is still noted. This suggests that the most important problem is that the model is predicting larger ε_t for the region between the peak ($x_2^+ = 11$) and $x_2^+ = 50$.

Acknowledgements

This work is supported by the DOE under grant DEFG02-86ER 13556. Computer resources have been provided by the National Center for Supercomputing Applications located at the University of Illinois.

References

Baik, S., Hanratty, T.J., 2003. Concentration profiles of droplets and prediction of the transition from stratified to annular flow in horizontal pipes. Int. J. Multiphase Flow 29, 329–338.

Binder, J.L., Hanratty, T.J., 1992. Use of Lagrangian statistics to describe drop deposition and distribution in horizontal gas liquid annular flows. Int. J. Multiphase Flow 18, 803–820.

Brooke, J.W., Hanratty, T.J., McLaughlin, J.B., 1994. Free-flight mixing and deposition of aerosols. Phys. Fluids 6, 3404–3415.

Caporaloni, M., Tampieri, F., Trombetti, F., Vittori, O., 1975. Transfer of particles in nonisotropic air turbulence. J. Atmos. Sci. 32, 565–568.

Chen, M., McLaughlin, J.B., 1995. A new correlation for the aerosol deposition rate in vertical ducts. J. Coll. Interf. Sci. 169, 437–455.

Clift, R., Grace, J.R., Weber, M.E., 1978. Bubbles, Drops and Particles. Academic Press, San Diego.
Du, S., Sawford, B.L., Wilson, J.D., Wilson, D.J., 1995. Estimation of the Kolmogorov constant (C_0) for the Lagrangian structure function, using a second-order Lagrangian model of grid turbulence. Phys. Fluids 7, 3083–3090.
Durbin, P.A., 1983. Stochastic differential equations and turbulent dispersion. NASA Reference Publication 1103.
Durbin, P.A., 1984. Comment on papers by Wilson et al. (1981) and Legg and Raupach (1982). Bound. Layer Meterol. 29, 409–411.
Hall, C.D., 1975. The simulation of particle motion in the atmosphere by a numerical random walk model. Q. J. R. Meterol. Soc. 101, 235–244.
Hanratty, T.J., 1956. Heat transfer through a homogeneous isotropic turbulent field. AIChE J. 2, 42–45.
Iliopoulos, I., Hanratty, T.J., 1999. Turbulent dispersion in a nonhomogeneous field. J. Fluid Mech. 392, 45–73.
Iliopoulos, I., Mito, Y., Hanratty, T.J., 2003. A stochastic model for solid particle dispersion in a nonhomogeneous turbulent field. Int. J. Multiphase Flow 29, 375–394.
Jones, W.P., Launder, B.E., 1972. The prediction of laminarization with a two-equation model of turbulence. Int. J. Heat Mass Transfer 15, 301–314.
Kontomaris, K., Hanratty, T.J., McLaughlin, J.B., 1992. An algorithm for tracking fluid particles in a spectral simulation of turbulent channel flow. J. Comput. Phys. 103, 231–242.
Legg, B.J., Raupach, M.R., 1982. Markov-chain simulation of particle dispersion in inhomogeneous flows: the mean drift velocity induced by a gradient in Eulerian velocity variance. Bound. Layer Meterol. 24, 3–13.
Lyons, S.L., Hanratty, T.J., McLaughlin, J.B., 1991. Large scale computer simulation of fully developed turbulent channel flow with heat transfer. Int. J. Numer. Meth. Fluids 13, 999–1028.
McCoy, D.D., Hanratty, T.J., 1977. Rate of deposition of droplets in annular two-phase flow. Int. J. Multiphase Flow 3, 319–331.
Mito, Y., Hanratty, T.J., 2002. Use of a modified Langevin equation to describe turbulent dispersion of fluid particles in a channel flow. Flow Turbul. Combust. 68, 1–26.
Monin, A.S., Yaglom, A.M., 1975. In: Statistical Fluid Mechanics, vol. 1. M.I.T. Press, Cambridge.
Pan, L., Hanratty, T.J., 2002. Correlation of entrainment for annular flow in horizontal pipes. Int. J. Multiphase Flow 28, 385–408.
Papavassiliou, D.V., Hanratty, T.J., 1997. Transport of a passive scalar in a turbulent channel flow. Int. J. Heat Mass Transfer 40, 1303–1311.
Paras, S.V., Karaberas, A.J., 1991. Droplet entrainment and deposition in horizontal annular flow. Int. J. Multiphase Flow 17, 455–468.
Perkins, R.J., 1992. The entrainment of heavy particles into a plane turbulent jet. In: Sommerfeld, M. (Ed.), Proceedings of the 6th workshop on two-phase flow predictions, Erlangen, pp. 18–33.
Pozorski, J., Minier, J.P., 1998. On the Lagrangian turbulent dispersion models based on the Langevin equation. Int. J. Multiphase Flow 24, 913–945.
Reeks, M.W., 1983. The transport of discrete particles in inhomogeneous turbulence. J. Aerosol Sci. 14, 729–739.
Reid, J.D., 1979. Markov chain simulations of vertical dispersion in the neutral surface layer for surface and elevated releases. Bound. Layer Meterol. 16, 3–22.
Reynolds, A.M., 1997. On the application of Thomson's random flight model to the prediction of particle dispersion within a ventilated airspace. J. Wind Eng. Ind. Aerodyn. 67–68, 627–638.
Sawford, B.L., 1991. Reynolds number effects in Lagrangian stochastic models of turbulent dispersion. Phys. Fluids A 3, 1577–1586.
Tennekes, H., 1979. The exponential Lagrangian correlation function and turbulent diffusion in the inertial subrange. Atmos. Environ. 13, 1565–1567.
Thomson, D.J., 1984. Random walk modelling of diffusion in inhomogeneous turbulence. Q. J. R. Meterol. Soc. 110, 1107–1120.
Thomson, D.J., 1986. A random walk model of dispersion in turbulent flows and its application to dispersion in a valley. Q. J. R. Meterol. Soc. 112, 511–530.
Thomson, D.J., 1987. Criteria for the selection of stochastic models of particle trajectories in turbulent flows. J. Fluid Mech. 180, 529–556.

van Dop, H., Nieuwstadt, F.T.M., Hunt, J.C.R., 1985. Random walk models for particle displacements in inhomogeneous unsteady turbulent flows. Phys. Fluids 28, 1639–1653.

Wang, Q., Squires, K.D., 1996. Large eddy simulation of particle deposition in a vertical turbulent channel flow. Int. J. Multiphase Flow 22, 667–683.

Wang, Q., Squires, K.D., Chen, M., McLaughlin, J.B., 1997. On the role of the lift force in turbulence simulations of particle deposition. Int. J. Multiphase Flow 23, 749–763.

Wilson, J.D., Thurtell, G.W., Kidd, G.E., 1981. Numerical simulation of particle trajectories in inhomogeneous turbulence, II: systems with variable turbulent velocity scale. Bound. Layer Meterol. 21, 423–441.